

Journal of Mechanics of Materials and Structures

**THICKNESS EFFECTS IN THE FREE VIBRATION OF
LAMINATED MAGNETOELECTROELASTIC PLATES**

Chao Jiang and Paul R. Heyliger

Volume 12, No. 4

July 2017



THICKNESS EFFECTS IN THE FREE VIBRATION OF LAMINATED MAGNETOELECTROELASTIC PLATES

CHAO JIANG AND PAUL R. HEYLIGER

A semianalytical discrete-layer approach is used to evaluate thickness effects in the free vibration of laminated magneto-electro-elastic (MEE) plates under various lateral boundary conditions. To match the primary physical phenomenon and simplify the study, piecewise continuous approximations are used through the thickness direction and either continuous global polynomial or trigonometric functions are used to simulate the deflection in axial or planar displacement fields. Thin plate models can be recovered to predict frequency estimation for various boundary conditions and compared with continuum-based theories using more complex approximations. Based on symmetry, the natural vibratory modes can be grouped to optimize computation. Numerical examples are used to show the thickness effects, with nondimensional frequencies computed for multiple plates under six lateral boundary conditions: simply supported, clamped, and four different combinations of free and clamped/simplely supported edges. Along with the influence of electroelastic and magnetoelastic coupling, the results of these analyses clearly illustrate the limits of thin-plate approximations.

Introduction

Kirchhoff's plate theory yields many exact solutions that can predict the behavior of elastic deformations and stresses near or across the interface of material layers under static and dynamic loading, but usually only when the planar dimensions are much larger than the thickness. These methods can also be used for solving more complicated situations for multilayered composites that are more complex than for homogeneous elastic materials. An example of this is a plate formed with materials that combine elastic, electric, and magnetic effects. These are typically referred to as magneto-electro-elastic (MEE) solids, and have behavior that is significantly different than the purely elastic case.

The free vibration of purely elastic laminated plates has a very rich history with numerous contributions, with one of the most significant being the early work of Srinivas et al. [1970]. The development of representative theories and solutions for laminates where the elastic fields are coupled with both magnetic and electric fields are much more recent. The free vibration of MEE plates has been investigated by several researchers. By expanding the general boundary conditions in series form, Vel and Batra [2000] solved the static deformation of multilayered piezoelectric plates using a three-dimensional solution. The corresponding bending vibration problem has been studied by Vel et al. [2004]. For a simply supported multilayered MEE plate, the exact free vibration behavior using an exact closed-form solution has been derived using the pseudo-Stroh formulation by Pan and Heyliger [2002]. The state-space formulation is another method that has been used to analyze the static and dynamic behavior of MEE multilayered plates [Wang et al. 2003; Chen et al. 2007]. This methodology was also used by Chen [Chen et al.

Keywords: thickness effects, free vibration, laminated, magneto-electro-elastic, plate.

2005] in the study of the free vibration of a nonhomogeneous isotropic MEE plate. Kondaiah, Shankar, and Ganesan [Kondaiah et al. 2012] used the finite element method to investigate beams made of MEE-thermo materials with different volume fractions under uniform temperature increase and clamped-free boundary conditions. The discrete-layer (DL) and domain-discretization methods have also been widely used in the analysis of anisotropic elastic and MEE plates and shells. The free vibration of an anisotropic and MEE plate was worked out by Chen, Heyliger and Pan [Chen et al. 2014] corresponding to different lateral boundary conditions.

The studies of many computational schemes for the solution of the equations of motion are based on the early work of Demarest [1971] and Eer Nisse [1967] through algorithms for elastic and piezoelectric parallelepipeds. However, if there is no existing closed-form solution, by expanding the displacements in terms of reasonable approximations, Hamilton's principle can be used to solve the weak form of the equations of motion. Furthermore, at an interface made of different materials, such as elastic, piezoelectric, and piezomagnetic properties, additional considerations may apply. Between two dissimilar materials, interface conditions include continuous stress, normal electric displacement, and normal magnetic induction. At a region of discontinuous material properties, these cause a discontinuity in the slope of the displacement and potential fields. The use of piecewise linear functions through the thickness with continuous global polynomial or trigonometric functions in the plane parallel to the interface allows a relatively accurate solution to be achieved. Via a semianalytical discrete-layer model, Heyliger [2000] developed the governing equations of layered elastic and piezoelectric parallelepipeds and obtained frequencies for a number of geometries and material combinations using this sort of approach.

Kirchhoff's classical theory of thin plates can often give sufficiently accurate results instead of carrying out a full three-dimensional stress analysis. But accuracy usually decreases with increasing thickness of the plate. Many authors qualify the value of the thickness relative to the larger plate dimensions as being "small" [Rao 2007], "much smaller" [Whitney 1987], or "significantly smaller" [Hjelmstad 1997]. Several authors have suggested limits with numbers attached: the thickness is "less than 1/20" [Ugural and Fenster 1995] of the lateral dimensions or that the lateral dimensions are "at least ten times" the thickness [Szilard 1974]. There has always been significant latitude assumed in applying these limits, since they are clearly influenced by plate geometry, the nature of the loading, and the material constitution. Such an inherent limitation of classical plate theory for the moderately thick plates necessitated the development of more refined theories in order to obtain reliable results for the behavior of these new materials. By plotting the frequencies as a function of the length-to-thickness ratio a/h , the present results indicate the level of errors influenced by thickness effects. The errors even within prior recommendations of a/h ratios can be significant.

The objective of this study is to use Hamilton's principle and appropriate approximations to make the link between the thin plate theory and more accurate continuum models to determine at what a/h ratios thin plate theory may be adequate for plates of laminated MEE material.

Theory

Governing equations. A plate is a structural element that is typically flat and thin. The lateral dimension is larger than the thickness by a factor that will be directly considered in this work. The plates considered in this study are formed by multiple anisotropic layers and all constitutive relations are linear. A

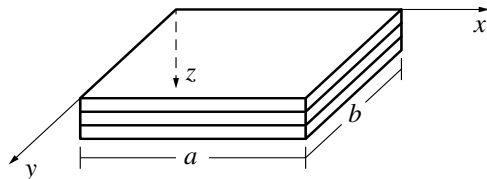


Figure 1. The geometry and coordinate system of the laminated plate.

rectangular Cartesian coordinate is used to formulate the governing equations with the origin as shown in Figure 1.

Of primary interest in this work are the thickness effects in laminated plate vibration for plates composed of MEE materials. Square laminates with lateral dimensions $a = b$ and a total thickness h are considered in this study. Each layer is homogeneous and each interface is perfectly bonded; therefore, the compatibility of displacements and the potentials are enforced. Even though the elastic displacements, electric and magnetic potentials, elastic traction, and the z -components of the electric displacement and magnetic induction are continuous, there is a discontinuity in the z -direction gradient of the displacement components, the electrostatic potential, and magnetostatic potential at the interface of two layers.

In a linear, isotropic MEE solid, the coupled constitutive law for each lamina can be expressed as

$$\sigma_{ij} = C_{ijkl}S_{kl} - e_{kij}E_k - q_{kij}H_k, \quad (1)$$

$$D_m = e_{mkl}S_{kl} + \epsilon_{mk}E_k + d_{mk}H_k, \quad (2)$$

$$B_m = q_{mkl}S_{kl} + d_{mk}E_k + \mu_{mk}H_k. \quad (3)$$

Here σ_{ij} , D_m , and B_m are respectively the components of stress, electric displacement, and magnetic induction; S_{kl} , E_k , and H_k represent the components of strain, electric field and magnetic field; C_{ijkl} , ϵ_{mk} , and μ_{mk} indicate the elastic, dielectric, and magnetic permeability coefficients; and e_{kij} , q_{kij} , and d_{mk} are the piezoelectric, piezomagnetic, and magnetoelectric coefficients. Moreover, by setting the values e_{mkl} or q_{mkl} equal to zero, the results for either purely piezoelectric, piezomagnetic, or elastic material can be achieved.

The relationship between the strain and displacement, electric (magnetic) field and its potential can be written as

$$S_{ij} = \frac{1}{2} \left(\frac{\partial u_i}{\partial x_j} + \frac{\partial u_j}{\partial x_i} \right), \quad (4)$$

$$E_k = -\frac{\partial \phi}{\partial x_k}, \quad (5)$$

$$H_k = -\frac{\partial \psi}{\partial x_k}. \quad (6)$$

Here, u_i are the infinitesimal displacement components and ϕ and ψ are the electric and magnetic potentials, respectively. The components x_k are related to the x , y and z in the rectangular Cartesian coordinates for $k = 1, 2, 3$.

The weak form of the equations of motion, the charge equation and the electromagnetic equation for a MEE medium within Hamilton's principle can be expressed as [Tiersten 1969]

$$\delta \int_{t_0}^t dt \int_V \left[\frac{1}{2} \rho \dot{u}_j \dot{u}_j - H(S_{kl}, E_k, H_k) \right] dV + \int_{t_0}^t dt \int_S (T_k \delta u_k - \sigma \delta \phi - I \delta \psi) dS = 0. \quad (7)$$

Here, t_0 and t are two specified times, V is the volume of the plate, S is the surface that bounds V , and δ is the variational operator. The \cdot superscript represents differentiation with respect to time, and T , σ , and I are surface tractions, surface charge, and surface current. H is the system enthalpy and can be written as

$$H = \frac{1}{2} C_{ijkl} S_{ij} S_{kl} - e_{ijk} E_i S_{jk} - \frac{1}{2} \epsilon_{ij} E_i E_j - q_{ijk} H_i S_{jk} - \frac{1}{2} \mu_{ij} H_i H_j - d_{ik} E_i H_k. \quad (8)$$

Based on the specific material properties used in this study, and setting $x_1 = x$, $x_2 = y$, and $x_3 = z$, with the corresponding displacement field as u , v , w , the weak form can be expanded as

$$\begin{aligned} & \int_{t_0}^t dt \int_V \left\{ \rho (\dot{u} \delta \dot{u} + \dot{v} \delta \dot{v} + \dot{w} \delta \dot{w}) \right. \\ & - \left[C_{11} \frac{\partial u}{\partial x} \frac{\partial \delta u}{\partial x} + C_{12} \frac{\partial u}{\partial x} \frac{\partial \delta v}{\partial y} + C_{12} \frac{\partial \delta u}{\partial x} \frac{\partial v}{\partial y} + C_{13} \frac{\partial u}{\partial x} \frac{\partial \delta w}{\partial z} \right. \\ & + C_{13} \frac{\partial \delta u}{\partial x} \frac{\partial w}{\partial z} + C_{22} \frac{\partial v}{\partial y} \frac{\partial \delta v}{\partial y} + C_{23} \frac{\partial v}{\partial y} \frac{\partial \delta w}{\partial z} + C_{23} \frac{\partial \delta v}{\partial y} \frac{\partial w}{\partial z} + C_{33} \frac{\partial w}{\partial z} \frac{\partial \delta w}{\partial z} \\ & + C_{16} \frac{\partial u}{\partial x} \left(\frac{\partial \delta u}{\partial y} + \frac{\partial \delta v}{\partial x} \right) + C_{16} \frac{\partial \delta u}{\partial x} \left(\frac{\partial u}{\partial y} + \frac{\partial v}{\partial x} \right) + C_{26} \frac{\partial v}{\partial y} \left(\frac{\partial \delta u}{\partial y} + \frac{\partial \delta v}{\partial x} \right) \\ & + C_{26} \frac{\partial \delta v}{\partial y} \left(\frac{\partial u}{\partial y} + \frac{\partial v}{\partial x} \right) + C_{36} \frac{\partial w}{\partial z} \left(\frac{\partial \delta u}{\partial y} + \frac{\partial \delta v}{\partial x} \right) + C_{36} \frac{\partial \delta w}{\partial z} \left(\frac{\partial u}{\partial y} + \frac{\partial v}{\partial x} \right) \\ & + C_{44} \left(\frac{\partial v}{\partial z} + \frac{\partial w}{\partial x} \right) \left(\frac{\partial \delta v}{\partial z} + \frac{\partial \delta w}{\partial x} \right) + C_{55} \left(\frac{\partial u}{\partial z} + \frac{\partial w}{\partial y} \right) \left(\frac{\partial \delta u}{\partial z} + \frac{\partial \delta w}{\partial y} \right) \\ & + C_{66} \left(\frac{\partial u}{\partial y} + \frac{\partial v}{\partial x} \right) \left(\frac{\partial \delta u}{\partial y} + \frac{\partial \delta v}{\partial x} \right) + C_{45} \left(\frac{\partial v}{\partial z} + \frac{\partial w}{\partial x} \right) \left(\frac{\partial \delta u}{\partial z} + \frac{\partial \delta w}{\partial y} \right) \\ & + C_{45} \left(\frac{\partial \delta v}{\partial z} + \frac{\partial \delta w}{\partial x} \right) \left(\frac{\partial u}{\partial z} + \frac{\partial w}{\partial y} \right) - e_{15} \delta E_1 \left(\frac{\partial u}{\partial z} + \frac{\partial w}{\partial x} \right) - e_{15} E_1 \left(\frac{\partial \delta u}{\partial z} + \frac{\partial \delta w}{\partial x} \right) \\ & - e_{24} \delta E_2 \left(\frac{\partial v}{\partial z} + \frac{\partial w}{\partial y} \right) - e_{24} E_2 \left(\frac{\partial \delta v}{\partial z} + \frac{\partial \delta w}{\partial y} \right) - e_{31} \delta E_3 \frac{\partial u}{\partial x} - e_{31} E_3 \frac{\partial \delta u}{\partial x} \\ & - e_{32} \delta E_3 \frac{\partial v}{\partial y} - e_{32} E_3 \frac{\partial \delta v}{\partial y} - e_{33} \delta E_3 \frac{\partial w}{\partial z} - e_{33} E_3 \frac{\partial \delta w}{\partial z} - q_{15} \delta H_1 \left(\frac{\partial u}{\partial z} + \frac{\partial w}{\partial x} \right) \\ & - q_{15} H_1 \left(\frac{\partial \delta u}{\partial z} + \frac{\partial \delta w}{\partial x} \right) - q_{24} \delta H_2 \left(\frac{\partial v}{\partial z} + \frac{\partial w}{\partial y} \right) - q_{24} H_2 \left(\frac{\partial \delta v}{\partial z} + \frac{\partial \delta w}{\partial y} \right) \\ & - q_{31} \delta H_3 \frac{\partial u}{\partial x} - q_{31} H_3 \frac{\partial \delta u}{\partial x} - q_{32} \delta H_3 \frac{\partial v}{\partial y} - q_{32} H_3 \frac{\partial \delta v}{\partial y} - q_{33} \delta H_3 \frac{\partial w}{\partial z} - q_{33} H_3 \frac{\partial \delta w}{\partial z} \\ & \left. - \epsilon_{11} E_1 \delta E_1 - \epsilon_{22} E_2 \delta E_2 - \epsilon_{33} E_3 \delta E_3 - \mu_{11} H_1 \delta H_1 - \mu_{22} H_2 \delta H_2 - \mu_{33} H_3 \delta H_3 \right] \Big\} dV \\ & + \int_{t_0}^t dt \int_S (T_k \delta u_k - \sigma \delta \phi - I \delta \psi) dS = 0. \quad (9) \end{aligned}$$

It is possible to integrate the weak form by parts and collect the coefficients with respect to δu , δv , δw , $\delta \phi$, and $\delta \psi$. Since we use the Ritz method, there is no need for this step. Here the focus is on the

quasistatic state, which means there is no electric charge or current densities across the surface. Body forces are also assumed to be zero in the results that follow.

Ritz approximations. The five primary field variables (u , v , w , ϕ , and ψ) can be approximated with x , y , z , and t as follows:

$$\begin{aligned}
 u(x, y, z, t) &= \sum_{j=1}^n U_j(x, y, t) \bar{\Psi}_j^u(z) = \sum_{i=1}^m \sum_{j=1}^n U_{ji}(t) \Psi_i^u(x, y) \bar{\Psi}_j^u(z), \\
 v(x, y, z, t) &= \sum_{j=1}^n V_j(x, y, t) \bar{\Psi}_j^v(z) = \sum_{i=1}^m \sum_{j=1}^n V_{ji}(t) \Psi_i^v(x, y) \bar{\Psi}_j^v(z), \\
 w(x, y, z, t) &= \sum_{j=1}^n W_j(x, y, t) \bar{\Psi}_j^w(z) = \sum_{i=1}^m \sum_{j=1}^n W_{ji}(t) \Psi_i^w(x, y) \bar{\Psi}_j^w(z), \\
 \phi(x, y, z, t) &= \sum_{j=1}^n \Phi_j(x, y, t) \bar{\Psi}_j^\phi(z) = \sum_{i=1}^m \sum_{j=1}^n \Phi_{ji}(t) \Psi_i^\phi(x, y) \bar{\Psi}_j^\phi(z), \\
 \psi(x, y, z, t) &= \sum_{j=1}^n \Psi_j(x, y, t) \bar{\Psi}_j^\psi(z) = \sum_{i=1}^m \sum_{j=1}^n \Psi_{ji}(t) \Psi_i^\psi(x, y) \bar{\Psi}_j^\psi(z).
 \end{aligned} \tag{10}$$

Here, U_{ji} , V_{ji} , W_{ji} , Φ_{ji} , and Ψ_{ji} are unknown constants. $\Psi_i(x, y)$ are the in-plane approximation functions, while $\bar{\Psi}_j$ are the one-dimensional Lagrangian interpolation polynomials in the thickness direction with respect to each variable.

The corresponding virtual fields can be expressed as

$$\begin{aligned}
 \delta u &= \Psi_i^u(x, y) \bar{\Psi}_j^u(z), \quad \delta v = \Psi_i^v(x, y) \bar{\Psi}_j^v(z), \quad \delta w = \Psi_i^w(x, y) \bar{\Psi}_j^w(z), \\
 \delta \phi &= \Psi_i^\phi(x, y) \bar{\Psi}_j^\phi(z), \quad \delta \psi = \Psi_i^\psi(x, y) \bar{\Psi}_j^\psi(z).
 \end{aligned} \tag{11}$$

By assuming periodic motion, substituting these approximations into the weak form, and collecting the coefficients of the variations of the displacements and placing the results in matrix form, the system can be written as

$$\begin{bmatrix} [M^{11}] & [0] & [0] & [0] & [0] \\ [0] & [M^{22}] & [0] & [0] & [0] \\ [0] & [0] & [M^{33}] & [0] & [0] \\ [0] & [0] & [0] & [0] & [0] \\ [0] & [0] & [0] & [0] & [0] \end{bmatrix} \begin{Bmatrix} \{U\} \\ \{V\} \\ \{W\} \\ \{\Phi\} \\ \{\Psi\} \end{Bmatrix} \rho \omega^2 = \begin{bmatrix} [K^{11}] & [K^{12}] & [K^{13}] & [K^{14}] & [K^{15}] \\ [K^{21}] & [K^{22}] & [K^{23}] & [K^{24}] & [K^{25}] \\ [K^{31}] & [K^{32}] & [K^{33}] & [K^{34}] & [K^{35}] \\ [K^{41}] & [K^{42}] & [K^{43}] & [K^{44}] & [K^{45}] \\ [K^{51}] & [K^{52}] & [K^{53}] & [K^{54}] & [K^{55}] \end{bmatrix} \begin{Bmatrix} \{U\} \\ \{V\} \\ \{W\} \\ \{\Phi\} \\ \{\Psi\} \end{Bmatrix}. \tag{12}$$

The submatrices here are related to the materials' characteristics, which include the elastic stiffnesses, piezoelectric coefficients, piezomagnetic coefficients, and shape functions. These matrices are given in the [Appendix](#).

The DL model is based on separating the field variables in the thickness direction and within the plane of the plate. This can effectively reduce the computational effort. One-dimensional Lagrangian polynomials are sufficient to describe these displacements in the thickness direction. The in-plane functions are generated depending on the various lateral boundary conditions. These are described below.

Boundary Conditions. The following classes of boundary conditions are discussed.

SSSS: simply supported around all edges. Srinivas [Srinivas et al. 1970] solved this problem using an exact method. The in-plane approximation functions are treated as harmonic functions, as per Heyliger [2000], to determine the fundamental in-plane modes.

For the simply supported condition,

$$w = \sigma_{xx} = \sigma_{xy} = \phi = \psi = 0 \quad \text{at } x = 0, a, \quad (13)$$

$$w = \sigma_{xy} = \sigma_{yy} = \phi = \psi = 0 \quad \text{at } y = 0, b. \quad (14)$$

To satisfy the essential boundary conditions on w , ϕ , and ψ , the in-plane approximations are

$$\Psi_i^u(x, y) = \cos \frac{m\pi x}{a} \sin \frac{n\pi y}{b}, \quad \Psi_i^v(x, y) = \sin \frac{m\pi x}{a} \cos \frac{n\pi y}{b}, \quad \Psi_i^w(x, y) = \sin \frac{m\pi x}{a} \sin \frac{n\pi y}{b}.$$

Here, ϕ and ψ have the same expression as w , and each individual pair of (m, n) contains a different value of i .

CCCC: clamped around all edges. The boundary conditions for this case are

$$u = v = w = \phi = \psi = 0 \quad \text{at } x = 0, a \quad \text{and at } y = 0, b. \quad (15)$$

Since displacements are zero at the domain endpoints, it is convenient to give the approximations along the (x, y) directions written in the “parent” domain (ξ, η) , which allows computations in terms of coordinate origins. Chen et al. [2014] used this approximation for all the clamped conditions and compared their results with frequencies from a FEM approach. The coordinates ξ and η are introduced as $\xi = 2x/a$ and $\eta = 2y/b$ and varying from -1 to 1 , with ξ_i and η_i being the equally spaced locations within $(-1, 1)$. For example, within the ξ domain, the displacements are expressed as following:

$$\text{when } i = 1, \quad f_x = (1 - \xi)(1 + \xi);$$

$$\text{when } i = 2, \quad f_x = (1 - \xi)\xi(1 + \xi);$$

$$\text{when } i = 3, \quad f_x = (1 - \xi)\left(\frac{1}{3} - \xi\right)\left(\frac{1}{3} + \xi\right)(1 + \xi).$$

FCFC: free-clamped-free-clamped. Here two opposite sides of the plate are “free” (in that all components of the stress-traction vector are 0, as are the electric displacement and normal flux), and the others are clamped. In this case it is assumed that the plate is clamped along the x direction, while the y direction is free. Therefore, the appropriate boundary conditions are

$$u = v = w = \phi = \psi = 0 \quad \text{at } x = 0, a, \quad (16)$$

$$\sigma_{yy} = \sigma_{xy} = \sigma_{yz} = D_y = B_y = 0 \quad \text{at } y = 0, b. \quad (17)$$

Demarest [1971] showed that group theory can be used to simplify vibration analysis in the case of traction-free surfaces using Legendre polynomials. The approximations are given in even/odd forms for these functions. The lowest three terms in the even group are 1 , $(3x^2 - 1)/2$, and $(35x^4 - 30x^2 + 3)/8$, while for the odd functions are shown as x , $(5x^3 - 3x)/2$, and $(63x^5 - 70x^3 + 15x)/8$ [Abromowitz and Stegun 1966].

CFFF: clamped-free-free-free. Here, only one edge is clamped; the others are free. This is also known as the cantilever plate; boundary conditions are as follows:

$$u = v = w = \phi = \psi = 0 \quad \text{at } x = 0, \quad (18)$$

$$\sigma_{xx} = \sigma_{xy} = \sigma_{xz} = D_x = B_x = 0 \quad \text{at } x = a, \quad (19)$$

$$\sigma_{yy} = \sigma_{xy} = \sigma_{yz} = D_y = B_y = 0 \quad \text{at } y = 0, b. \quad (20)$$

Here, to match the displacements at $x = 0$, we use power series of at least first order along the x direction and maintain the Legendre polynomials in the y direction.

CCFF: clamped-clamped-free-free. Here two adjacent edges are clamped, while the others are free; boundary conditions are as follows:

$$u = v = w = \phi = \psi = 0 \quad \text{at } x = 0, y = 0, \quad (21)$$

$$\sigma_{xx} = \sigma_{xy} = \sigma_{xz} = D_x = B_x = 0 \quad \text{at } x = a, \quad (22)$$

$$\sigma_{yy} = \sigma_{xy} = \sigma_{yz} = D_y = B_y = 0 \quad \text{at } y = b. \quad (23)$$

The displacements and potential along the x and y directions are extended as power series in a manner similar to the cantilever plate.

SFSF: simple-free-simple-free. In this condition, two opposite sides are simply supported and the others are free; boundary conditions are as follows:

$$w = \sigma_{xx} = \sigma_{xy} = \phi = \psi = 0 \quad \text{at } x = 0, a, \quad (24)$$

$$\sigma_{yy} = \sigma_{xy} = \sigma_{yz} = D_y = B_y = 0 \quad \text{at } y = 0, b. \quad (25)$$

Fourier series are used in the x direction. The only difference is specified terms for the approximate function, as m and n are either $2i + 1$ or $2i$. The approximation functions in u and v are coupled with the displacement in w , and the modes are separated into two groups (odd and even) according to these groupings. For example, the first terms in odd group are: $\Psi_1^u(x, y) = \cos(\pi x/a) \sin(\pi y/b)$, $\Psi_1^v(x, y) = \sin(\pi x/a) \cos(\pi y/b)$, and $\Psi_1^w(x, y) = \sin(\pi x/a) \sin(\pi y/b)$. The first terms in the even group are: $\Psi_2^u(x, y) = \cos(2\pi x/a) \sin(2\pi y/b)$, $\Psi_2^v(x, y) = \sin(2\pi x/a) \cos(2\pi y/b)$, and $\Psi_2^w(x, y) = \sin(2\pi x/a) \sin(2\pi y/b)$. For all clamped-clamped and clamped-free conditions, symmetry can be used to exploit the nature of the eigenvalue problem. By grouping the approximations according to symmetry groups as introduced by Ohno [1976], the original complete problem can be reduced into four smaller problems with the same result but at a lower computational cost.

Results

Isotropic plates. Several problems are first considered for the homogeneous isotropic plate to demonstrate the accuracy of the DL model. This type of plate has a number of solutions with which to compare.

Simply supported condition. The convergence of the semianalytical discrete layer model has been explored using the natural frequencies of a square isotropic plate. For the simply supported condition, the Navier solution gives an exact result for Kirchhoff's plate theory. The in-plane variations in transverse displacement are given as a single term in the sine or cosine components of the expansion. Fixing $a/b = 1$,

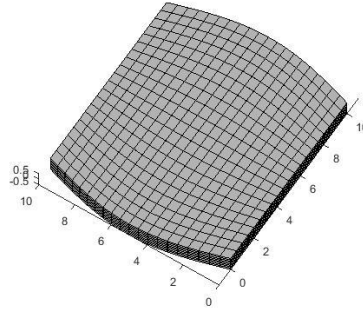


Figure 2. The first in-plane mode of the SSSS isotropic plate (mode 7).

$a/h = 10$, and $\nu = 0.3$, the natural frequencies are compared with Srinivas’s elasticity theory and Reddy’s higher-order shear deformation theory (HSDPT) [Reddy and Phan 1985].

Equal thicknesses of each discrete layer were used. The results are presented in terms of the nondimensional parameter $\bar{\omega} = \omega(\rho h^2/G)^{1/2}$. Each frequency was computed using 36 in-plane terms and eight sublayers, which gave values of sufficient accuracy such that little change was observed in increasing the numbers beyond these limits. The results are shown in Table 1. The highlights in bold indicate the in-plane modes for which the transverse displacement is zero. The mode shapes for the bending modes are well known and are not repeated here. The seventh mode, which is purely in-plane and is not included or computed by Srinivas or Reddy, is shown in Figure 2 and is an example of the usefulness of continuum theories that provide all modes rather than just those related to bending.

All-clamped condition. The natural frequencies of an all clamped isotropic ($\nu = 0.3$) plate have been computed by Liew et al. [1993] using the Rayleigh–Ritz procedure to solve the energy function derived from Mindlin’s plate theory. The frequency parameter was given as $\bar{\omega} = (\omega a^2/\pi^2)\sqrt{\rho h/D}$, where $D = Eh^3/[12(1 - \nu^2)]$ and h is the total thickness. Using 36 in-plane terms with eight layers, results are shown in Table 2. Once again, the present model captures in-plane modes (listed in bold face) that were not considered by the previous authors. It is clear that as the thickness increases, the in-plane frequencies are reduced and approach the lowest bending frequency given by simpler theories.

frequency number	[Srinivas et al. 1970]	HSDPT [Reddy and Phan 1985]	present solution		
			$N = 4$	$N = 8$	$N = 16$
1	0.0932	0.0931	0.0939	0.0933	0.0932
2, 3	0.226	0.2222	0.2245	0.2231	0.2227
4	0.3421	0.3411	0.3452	0.3429	0.3423
5, 6	0.4171	0.4158	0.4211	0.4182	0.4174
7	–	–	0.4443	0.4443	0.4443
8, 9	0.5239	0.5221	0.5292	0.5253	0.5243
10	–	0.6545	0.6642	0.6589	0.6575

Table 1. The first ten nondimensional frequencies of an isotropic square plate under the simply supported boundary condition (SSSS) with $\nu = 0.3$ and $a/h = 10$, normalized by $\bar{\omega} = \omega(\rho h^2/G)^{1/2}$.

frequency number	$a/h = 10$		$a/h = 5$	
	[Liew et al. 1993]	present	[Liew et al. 1993]	present
1	3.2954	3.3297	2.6875	2.7370
2	6.2858	6.3633	4.6907	4.7940
3	6.2858	6.3633	4.6907	4.7940
4	8.8098	8.9295	–	6.2751
5	10.3788	10.5316	–	6.2751
6	10.4778	10.6316	6.2985	6.4484
7	–	12.5221	7.1767	7.3598
8	–	12.5221	–	7.4371
9	12.5529	12.7474	7.2759	7.4621
10	12.5529	12.7474	8.5155	8.7416

Table 2. The first ten nondimensional frequencies of an isotropic square plate under the CCCC boundary condition with $\nu = 0.3$, normalized by $\bar{\omega} = (\omega a^2 / \pi^2) \sqrt{\rho h / D}$.

frequency number	$a/h = 10$		$a/h = 5$	
	[Liew et al. 1993]	present	[Liew et al. 1993]	present
1	2.0904	2.1094	1.7772	1.8061
2	2.4342	2.4533	2.0151	2.0429
3	3.9055	3.9312	–	2.9771
4	5.3392	5.3996	3.1652	3.2004
5	5.7811	5.8408	4.0413	4.1242
6	–	5.9501	4.3472	4.4262
7	6.9368	6.9834	–	5.3326
8	7.3046	7.3757	–	5.4493
9	9.6241	9.7567	5.3813	5.4827
10	9.9989	10.0960	5.3813	5.4831

Table 3. The first ten nondimensional frequencies of an isotropic square plate under the FCFC boundary condition with $\nu = 0.3$, normalized by $\bar{\omega} = (\omega a^2 / \pi^2) \sqrt{\rho h / D}$.

FCFC condition. Table 3 lists the first ten nondimensional natural frequencies of isotropic square plates for the FCFC condition. This case was also considered by Liew et al. [1993] and the DL results provide frequency predictions that are close to but slightly above those numbers.

CFFF condition. The cantilever plate is an extremely important case that has numerous practical applications. Liew et al. [1993] gave results without showing the mode shapes. Frequencies are given in Table 4. The present model again consistently gives bending and torsional frequencies that are slightly larger than those of the Mindlin results compared to the previous work. The in-plane frequencies are normally smaller.

CCFF Condition. Results for this case are computed using four terms in both x and y directions together with four layers through the thickness. Comparison of frequencies is demonstrated in Table 5 and indicate

frequency number	$a/h = 10$		$a/h = 5$	
	[Liew et al. 1993]	present	[Liew et al. 1993]	present
1	0.3476	0.3573	0.3384	0.3471
2	0.8168	0.8401	0.7445	0.7637
3	2.0356	2.1111	–	1.1181
4	2.5836	2.2349	1.7806	1.8451
5	2.8620	2.9795	2.2765	2.5154
6	4.8162	3.0007	2.4205	2.5742
7	5.4834	5.3357	3.8851	2.6689
8	5.7769	5.4769	4.3168	2.9809
9	6.2381	5.9619	4.5996	4.3811
10	7.9181	7.9682	4.8966	4.8979

Table 4. The first ten nondimensional frequencies of an isotropic square plate under the CFFF boundary condition with $\nu = 0.3$, normalized by $\bar{\omega} = (\omega a^2 / \pi^2) \sqrt{\rho h / D}$.

frequency number	$a/h = 10$		$a/h = 5$	
	[Liew et al. 1993]	present	[Liew et al. 1993]	present
1	0.6762	0.6946	0.6328	0.6489
2	2.2438	2.3246	1.9221	1.9856
3	2.5049	2.6055	2.1499	2.2313
4	4.2557	4.5059	–	2.6032
5	5.5633	5.2043	–	3.3287
6	5.8188	6.6564	3.4217	3.5729
7	7.2399	7.9353	4.3468	3.9720
8	7.5055	7.9449	4.5533	5.3123
9	9.9651	8.6372	5.4276	5.6800
10	10.1661	9.5767	5.6539	6.1263

Table 5. The first ten nondimensional frequencies of an isotropic square plate under the CCFF boundary condition with $\nu = 0.3$, normalized by $\bar{\omega} = (\omega a^2 / \pi^2) \sqrt{\rho h / D}$.

slightly larger discrepancies that those of prior predictions. Some of this may be differences in actual bending frequencies, but other gaps may exist because the model of Liew et al. [1993] may not capture some of the nonbending modes, especially as the plate becomes thick.

SFSF condition. Table 6 shows the comparison with Liew et al.'s results [1993]. It again appears that the model of the previous authors captures only the bending frequencies under the SFSF condition. Hence at a minimum, the lower modes can be directly compared.

Composite MEE plates. There are three primary features associated with the results in this section. The first is a direct comparison with one of the few models of laminated MEE plates to ensure accuracy of the results that follow. The second is a collection of results for laminated MEE plates under a variety of

frequency number	$a/h = 10$		$a/h = 5$	
	[Liew et al. 1993]	present	[Liew et al. 1993]	present
1	0.9565	0.9593	0.9102	0.9139
2	1.5593	1.5670	1.4280	1.4342
3	3.4307	3.4808	–	2.4697
4	3.6838	3.7036	2.9521	2.9845
5	4.3358	4.3634	3.1684	3.1994
6	–	4.9400	3.6435	3.6777
7	6.2971	6.4010	–	4.6127
8	6.7071	6.9051	5.0216	5.0994
9	7.7648	7.8291	5.3173	5.4507
10	8.3513	8.4230	–	5.6993

Table 6. The first ten nondimensional frequencies of an isotropic square plate under SFSF boundary condition with $\nu = 0.3$, normalized by $\bar{\omega} = (\omega a^2/\pi^2)\sqrt{\rho h/D}$.

CCCC	[Chen et al. 2014]	present	FCFC	[Chen et al. 2014]	present
1	0.3332	0.3332	1	0.2193	0.2193
2	0.5987	0.5987	2	0.2572	0.2572
3	0.5987	0.5987	3	0.3798	0.3798
4	0.7459	0.7459	4	0.3967	0.3967
5	0.7459	0.7459	5	0.5182	0.5182
6	0.8138	0.8138	6	0.5656	0.5656

Table 7. The first six nondimensional frequencies of an elastic square plate with hexagonal materials under CCCC and FCFC conditions, normalized by $\bar{\omega} = \omega h\sqrt{\rho/C_{11}}$.

lamination schemes and boundary conditions. Finally, the influence of the a/h ratio on the frequencies for these plates are explored.

Comparison with existing results. The free vibration of composite MEE plates under CCCC and FCFC conditions has been extensively studied by Chen, Heyliger and Pan [Chen et al. 2014] for a fixed a/h ratio. These simulations all used properties for either a purely elastic hexagonal material, the piezoelectric material barium titanate (BaTiO_3), denoted in this work by the letter B, and the magnetostrictive material cobalt ferrite (CoFe_2O_4), denoted in this study by the letter F. All plates are assumed to have three layers of equal thickness. In the case of homogeneous MEE materials, either BBB or FFF are used to denote the differing materials. Composites use FBF or BFB to indicate the lamination scheme. The material properties are given in [Chen et al. 2014]. These results were repeated here to ensure accuracy for MEE media and are summarized in Table 7. Excellent agreement was found for all cases.

For the remaining examples, the nondimensional frequencies are calculated by $\bar{\omega} = \omega h\sqrt{\rho_{\max}/c_{\max}}$ and are typically plotted using the parameter $\Omega = \bar{\omega}(a^2/h)\sqrt{\rho_{\max}/c_{\max}}$. Here ρ_{\max} is the largest value of material density in the laminate and c_{\max} is the largest component of the elastic stiffness tensor in the laminate.

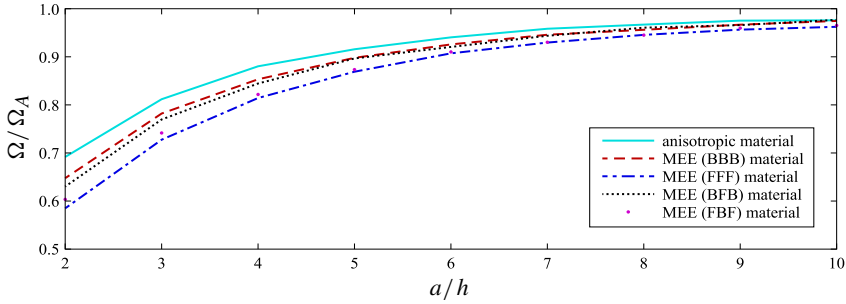


Figure 3. The relative differences of fundamental frequencies of the SSSS plate compared to the thin plate limit for the five different material combinations as a function of a/h .

SSSS condition. The influence of a/h for very thick plates was first studied for the five basic lamination schemes (hexagonal, BBB, FFF, FBF, and BFB). In this case, all frequencies were normalized by their respective values for the thin plate, taken as the frequency computed at $a/h = 30$. Beyond this point there was very little change in the dimensionless frequency for all plates considered. The results of this analysis are shown in Figure 3 for the fundamental frequency and show that the level of difference with thin plate limits are ordered as FFF > FBF > BFB > BBB > hex. Hence the purely magnetostrictive plate has stronger thickness effects than the purely elastic hexagonal plate.

Figure 4 displays the influence of slenderness for the first six frequencies of a hexagonal material along with the corresponding mode shapes. It appears that there are only four curves, but this is because

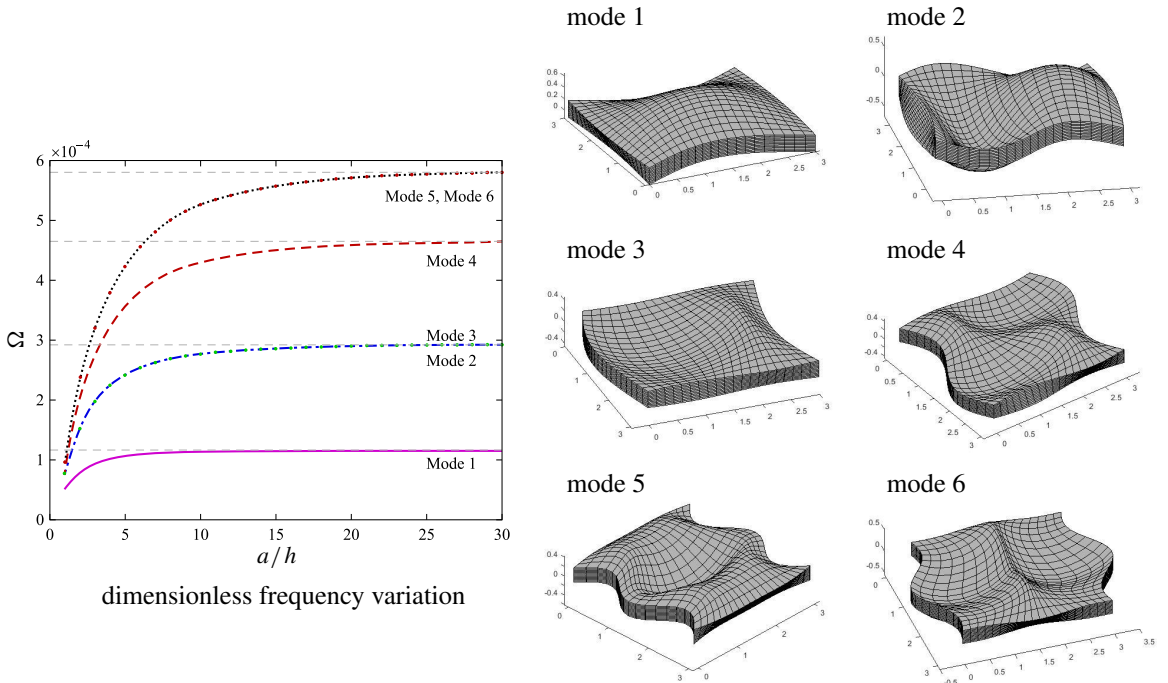


Figure 4. Frequency variation as a function of a/h and the first six mode shapes ($a/h = 10$) for the anisotropic elastic square SSSS plate.

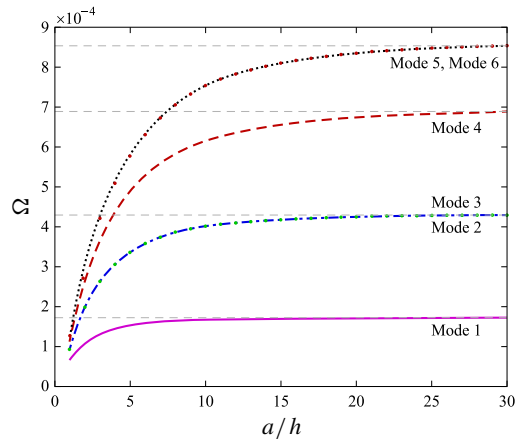


Figure 5. Dimensionless frequency variation as a function of a/h for the SSSS square BFB plate.

frequencies	B material		F material	
	[Chen et al. 2014]	present	[Chen et al. 2014]	present
1	1.7817	1.7817	1.3667	1.3667
2	2.9486	2.9486	2.2311	2.2311
3	2.9486	2.9486	2.2311	2.2311
4	3.2195	3.2195	2.7905	2.7905
5	3.2195	3.2195	2.2311	2.2311
6	3.7120	3.7120	2.9345	2.9345

Table 8. The first six nondimensional frequencies of square plates composed of BBB and FFF materials under the CCCC condition, normalized by $\bar{\omega} = \omega a \sqrt{\rho_{\max}/C_{\max}}$.

several of the modes for this boundary condition are repeated. The horizontal dashed lines indicate the asymptote of each frequency which is again chosen using the value at $a/h = 30$. **Figure 5** shows the frequency arrangement of BFB materials. The arrangements are similar for other stacking sequences. The character of all of the curves are very similar in nature, with slight differences in value and mode order sometimes occurring. **Table 9** lists the first six frequencies at a/h ratios of 30 for reference since these values are used for all plots and can be used as thin plate predictions using other models. As was the case for the very thick plates, an increased amount of F material results in larger differences in the thin plate limits. Yet for an a/h ratio larger than 20, the differences are within 3 percent.

CCCC condition. The differences of the first frequency with respect to a/h for the five stacking sequences are shown in **Figure 6**. The differences between the thin-plate limits are all slightly higher than those of the SSSS condition, with differences of about 10 percent when $a/h = 10$. **Figure 7** gives the first six frequencies of the hexagonal plate as a function of a/h ratio and the corresponding mode shapes. It is clear that as the slenderness increases, the fifth and the sixth frequencies are identical.

bending mode	hex	BBB	FFF	BFB	FBF
1	$1.17 \cdot 10^{-4}$	$2.92 \cdot 10^{-4}$	$1.83 \cdot 10^{-4}$	$1.73 \cdot 10^{-4}$	$1.97 \cdot 10^{-4}$
2	$2.92 \cdot 10^{-4}$	$7.24 \cdot 10^{-4}$	$4.55 \cdot 10^{-4}$	$4.31 \cdot 10^{-4}$	$4.88 \cdot 10^{-4}$
3	$2.92 \cdot 10^{-4}$	$7.24 \cdot 10^{-4}$	$4.55 \cdot 10^{-4}$	$4.31 \cdot 10^{-4}$	$4.88 \cdot 10^{-4}$
4	$4.65 \cdot 10^{-4}$	$1.16 \cdot 10^{-3}$	$7.24 \cdot 10^{-4}$	$6.88 \cdot 10^{-4}$	$7.79 \cdot 10^{-4}$
5	$5.79 \cdot 10^{-4}$	$1.44 \cdot 10^{-3}$	$9.01 \cdot 10^{-4}$	$8.52 \cdot 10^{-4}$	$9.68 \cdot 10^{-4}$
6	$5.79 \cdot 10^{-4}$	$1.44 \cdot 10^{-3}$	$9.01 \cdot 10^{-4}$	$8.52 \cdot 10^{-4}$	$9.68 \cdot 10^{-4}$

Table 9. Frequencies for homogeneous plates composed of five stacking sequences under the SSSS condition at $a/h = 30$.

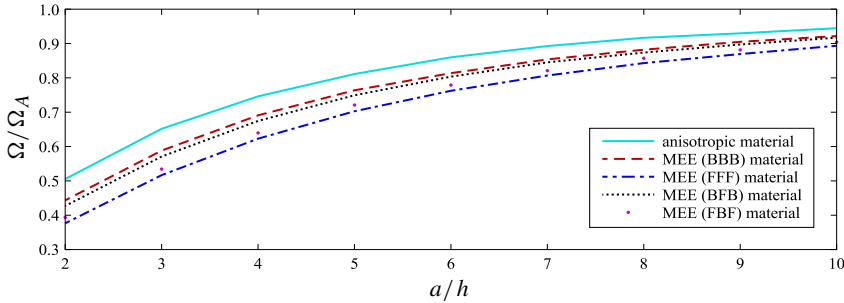


Figure 6. The relative differences of fundamental frequencies of the CCCC plate compared to the thin plate limit for the five different material combinations as a function of a/h .

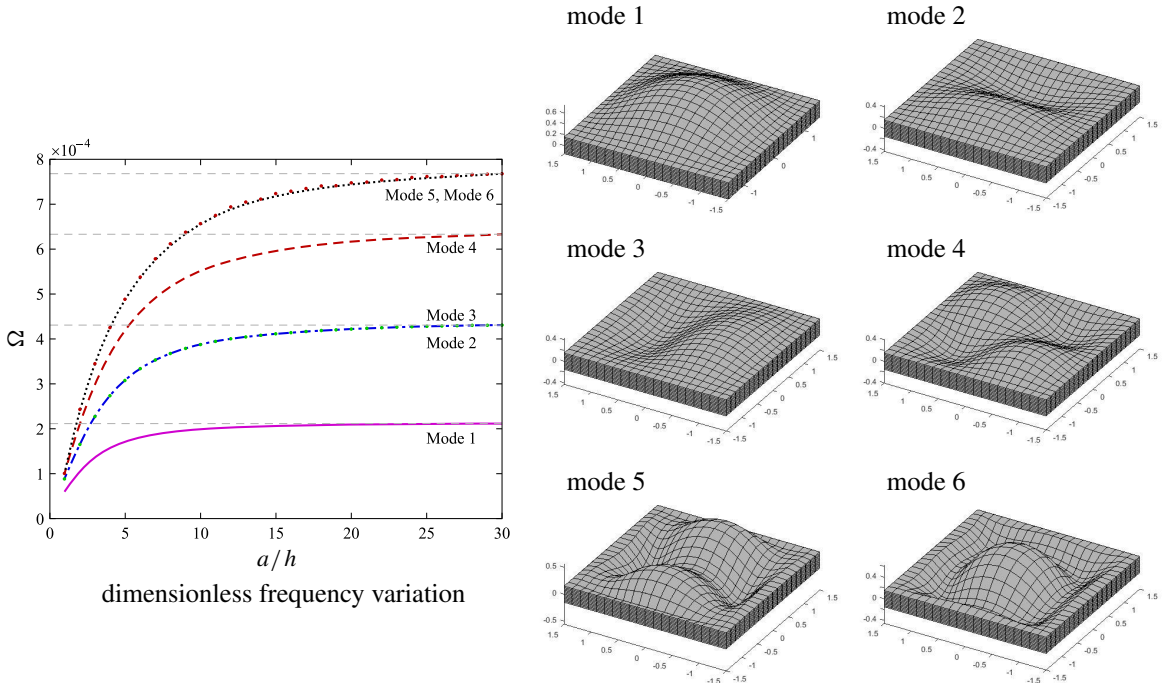


Figure 7. Frequency variation as a function of a/h and the first six mode shapes ($a/h = 10$) for the anisotropic elastic square CCCC plate.

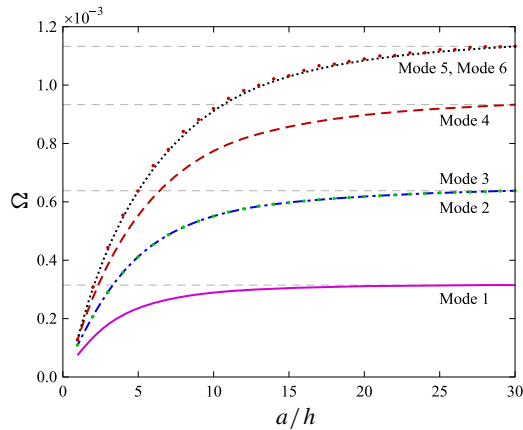


Figure 8. Dimensionless frequency variation as a function of a/h for the CCCC square BFB plate.

bending mode	hex	BBB	FFF	BFB	FBF
1	$2.12 \cdot 10^{-4}$	$5.32 \cdot 10^{-4}$	$3.37 \cdot 10^{-4}$	$3.16 \cdot 10^{-4}$	$3.61 \cdot 10^{-4}$
2	$4.31 \cdot 10^{-4}$	$1.07 \cdot 10^{-3}$	$6.76 \cdot 10^{-4}$	$6.39 \cdot 10^{-4}$	$7.24 \cdot 10^{-4}$
3	$4.31 \cdot 10^{-4}$	$1.07 \cdot 10^{-3}$	$6.76 \cdot 10^{-4}$	$6.39 \cdot 10^{-4}$	$7.24 \cdot 10^{-4}$
4	$6.33 \cdot 10^{-4}$	$1.57 \cdot 10^{-3}$	$9.86 \cdot 10^{-4}$	$9.31 \cdot 10^{-4}$	$1.06 \cdot 10^{-3}$
5	$7.67 \cdot 10^{-4}$	$1.90 \cdot 10^{-3}$	$1.19 \cdot 10^{-3}$	$1.13 \cdot 10^{-3}$	$1.28 \cdot 10^{-3}$
6	$7.67 \cdot 10^{-4}$	$1.92 \cdot 10^{-3}$	$1.20 \cdot 10^{-3}$	$1.13 \cdot 10^{-3}$	$1.29 \cdot 10^{-3}$

Table 10. Frequencies for homogeneous plates composed of five stacking sequences under the CCCC condition at $a/h = 30$.

Figure 8 shows the effect of the length-to-thickness ratio for the first six frequencies for BFB plates under all-clamped conditions. The levels of difference with the thin-plate limits are similar to those of the fully simply supported condition. Frequencies are repeated and lines are coincident for modes 2 and 3. Table 10 lists the first six frequencies of the five stacking sequences under the all-clamped condition with a/h equal to 30.

FCFC condition. Figure 9 shows the frequency response for the five stacking sequences under the FCFC condition. Figure 10 shows the influence of a/h ratio for the hexagonal material along with the lowest six mode shapes. Figure 11 gives the slenderness effects for BFB materials. Table 11 gives the values of the first seven frequencies according to five stacking sequences at slenderness of $a/h = 30$. Reductions are smaller for the piezoelectric and piezomagnetic plates in the sixth frequency. This is apparent from the different curvature of each frequency lines. As a/h ratios approach 20, the percentage differences are within 5 percent.

CFFF condition. Figure 12 shows the difference of the five stacking sequences with respect to the fundamental frequency. Reductions are less variable under this condition than several other support conditions. Even with $a/h = 10$, the BFB plate still maintains a 5 percent reduction from the thin-plate estimates.

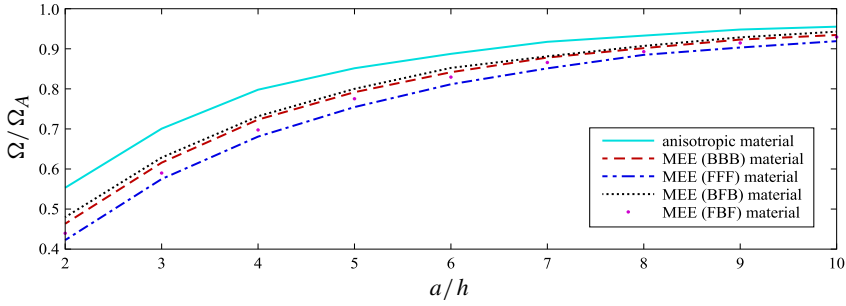


Figure 9. The relative differences of fundamental frequencies of the FCFC plate compared to the thin plate limit for the five different material combinations as a function of a/h .

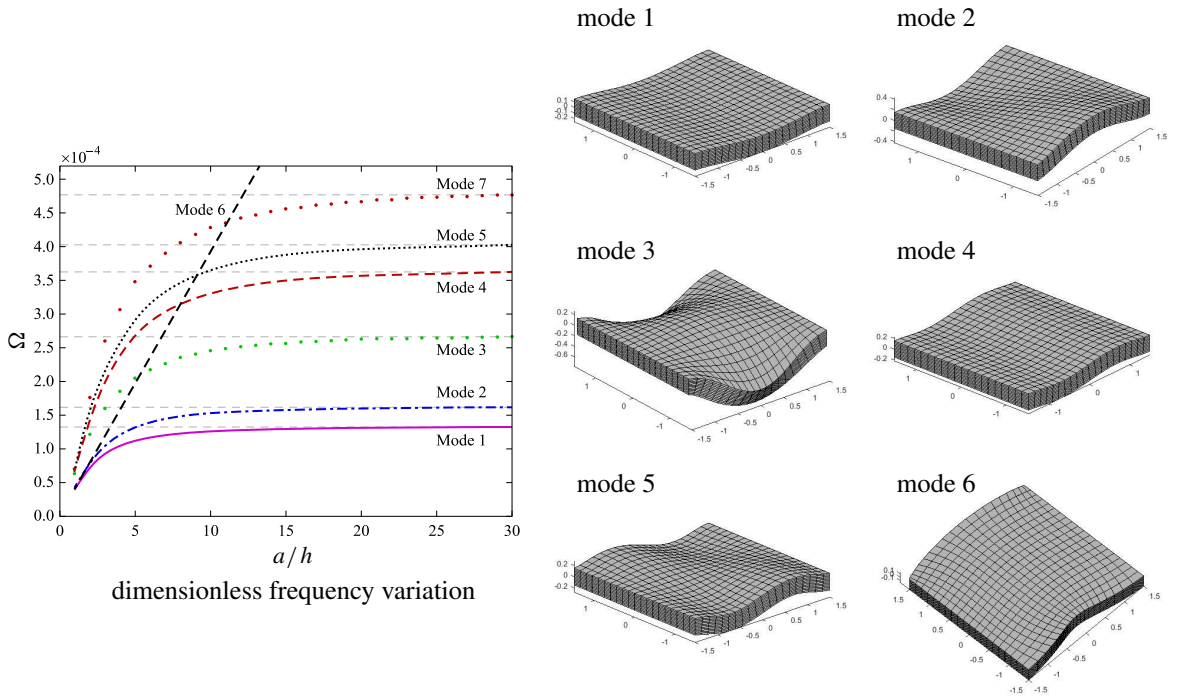


Figure 10. Frequency variation as a function of a/h and the first six mode shapes ($a/h = 10$) for the anisotropic elastic square FCFC plate.

bending mode	hex	BBB	FFF	BFB	FBF
1	$1.33 \cdot 10^{-4}$	$3.20 \cdot 10^{-4}$	$2.07 \cdot 10^{-4}$	$1.94 \cdot 10^{-4}$	$2.22 \cdot 10^{-4}$
2	$1.62 \cdot 10^{-4}$	$3.77 \cdot 10^{-4}$	$2.42 \cdot 10^{-4}$	$2.28 \cdot 10^{-4}$	$2.59 \cdot 10^{-4}$
3	$2.67 \cdot 10^{-4}$	$6.21 \cdot 10^{-4}$	$3.96 \cdot 10^{-4}$	$3.74 \cdot 10^{-4}$	$4.25 \cdot 10^{-4}$
4	$3.63 \cdot 10^{-4}$	$8.70 \cdot 10^{-4}$	$5.62 \cdot 10^{-4}$	$5.30 \cdot 10^{-4}$	$6.04 \cdot 10^{-4}$
5	$4.03 \cdot 10^{-4}$	$9.49 \cdot 10^{-4}$	$6.09 \cdot 10^{-4}$	$5.76 \cdot 10^{-4}$	$6.57 \cdot 10^{-4}$
6	$4.77 \cdot 10^{-4}$	$1.13 \cdot 10^{-3}$	$7.24 \cdot 10^{-4}$	$6.88 \cdot 10^{-4}$	$7.79 \cdot 10^{-4}$

Table 11. Frequencies for homogeneous plates composed of five stacking sequences under the FCFC condition at $a/h = 30$.

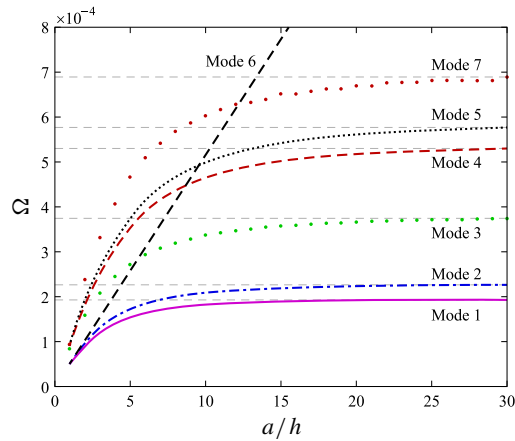


Figure 11. Dimensionless frequency variation as a function of a/h for the FCFC square BFB plate.

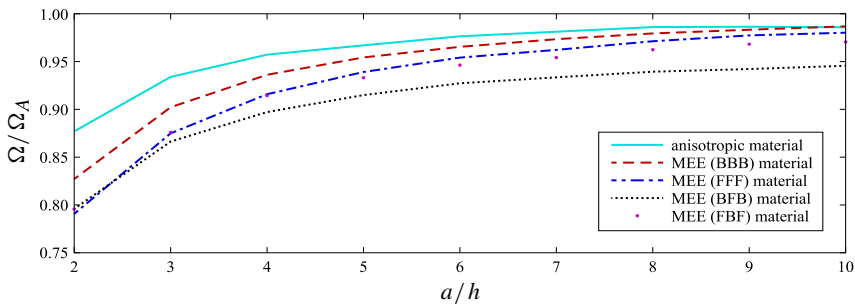


Figure 12. The relative differences of fundamental frequencies of the CFFF plate compared to the thin plate limit for the five different material combinations as a function of a/h .

Figure 13 displays the first eight frequencies as a function of a/h ratio and the first six mode shapes under CFFF condition. Once again the straight dashed lines represent the in-plane modes. The mode shapes are almost the same as isotropic plates under this boundary condition. Figure 14 gives the configuration of frequencies of the BFB stacking sequence. Table 12 lists the frequency values of the first six bending modes at $a/h = 30$. The differences are quite small for this condition, with the percent difference being below 10 percent even up to the fifth frequency with $a/h = 10$. When the length-to-thickness ratio is 20, the sixth frequency reductions are nearly 2 percent.

CCFF condition. Figure 15 demonstrates the reduction for the lowest frequency for various a/h ratios. At a/h of 6, percent differences are within 10 percent for each material. Figure 16 shows the first nine frequencies and the first six mode shapes of the plates made of anisotropic materials under CCFF condition. More in-plane modes appear within these bending frequencies than for prior conditions, indicating increased stiffening in bending. Figure 17 gives the influence of slenderness for the first nine frequencies for the plate composed with BFB materials. Even as a/h is equal to 20, the reductions are still over 5 percent. Table 13 gives the first six modes at $a/h = 30$ for reference.

SFSF condition. Figure 18 shows the differences of the fundamental frequency for the five cases. This

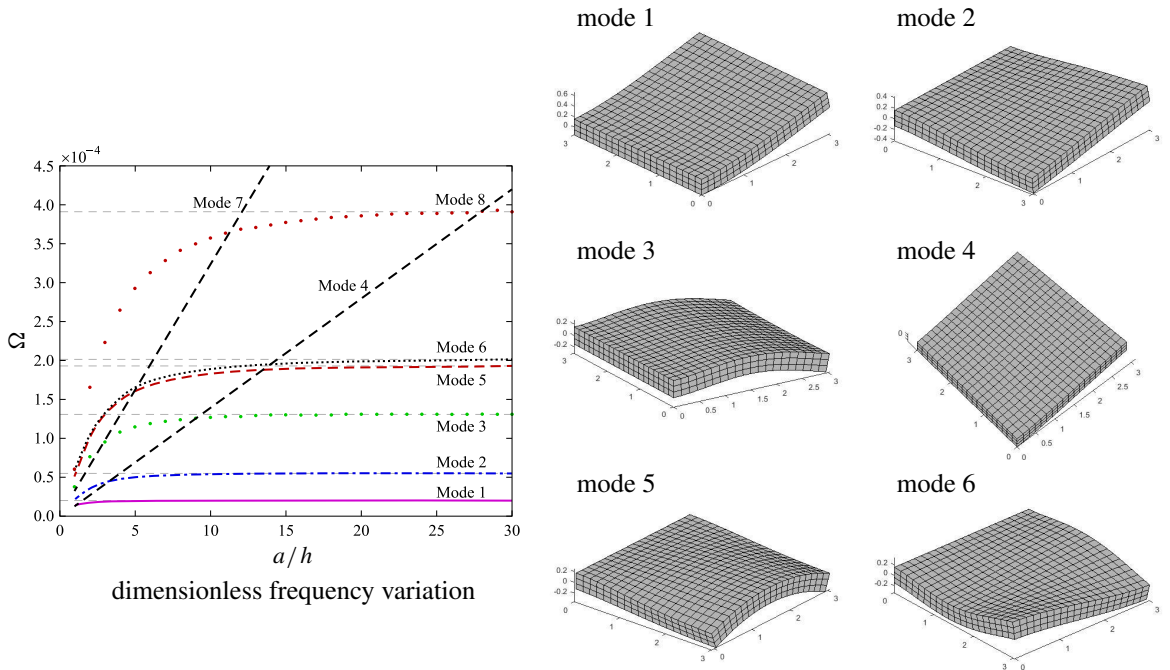


Figure 13. Frequency variation as a function of a/h and the first six mode shapes ($a/h = 10$) for the anisotropic elastic square CFFF plate.

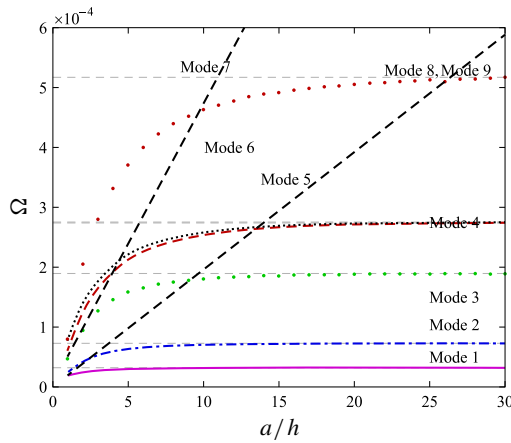


Figure 14. Dimensionless frequency variation as a function of a/h for the CFFF square BFB plate.

configuration is similar to the all simply supported condition; however, reductions are slightly smaller for the same a/h conditions. Figure 19 demonstrates the configuration of the first seven frequencies and the first six modes of anisotropic materials under SFSF condition. The straight dashed line corresponds to the in-plane mode 6. Figure 20 shows frequency variation as a function of a/h . These are almost the same as those for anisotropic plates except that the difference between the third and fourth bending frequencies, which are the bending modes along simply supported edges and the bending mode along

bending mode	hex	BBB	FFF	BFB	FBF
1	$2.09 \cdot 10^{-5}$	$5.19 \cdot 10^{-5}$	$3.45 \cdot 10^{-5}$	$3.29 \cdot 10^{-5}$	$3.72 \cdot 10^{-5}$
2	$5.57 \cdot 10^{-5}$	$1.22 \cdot 10^{-4}$	$7.85 \cdot 10^{-5}$	$7.30 \cdot 10^{-5}$	$8.40 \cdot 10^{-5}$
3	$1.31 \cdot 10^{-4}$	$3.15 \cdot 10^{-4}$	$2.08 \cdot 10^{-4}$	$1.90 \cdot 10^{-4}$	$2.22 \cdot 10^{-4}$
4	$1.93 \cdot 10^{-4}$	$4.58 \cdot 10^{-4}$	$2.96 \cdot 10^{-4}$	$2.74 \cdot 10^{-4}$	$3.17 \cdot 10^{-4}$
5	$2.01 \cdot 10^{-4}$	$4.53 \cdot 10^{-4}$	$2.95 \cdot 10^{-4}$	$2.75 \cdot 10^{-4}$	$3.13 \cdot 10^{-4}$
6	$3.91 \cdot 10^{-4}$	$8.58 \cdot 10^{-4}$	$5.48 \cdot 10^{-4}$	$5.17 \cdot 10^{-4}$	$5.87 \cdot 10^{-4}$

Table 12. Frequencies for homogeneous plates composed of five stacking sequences under the CFFF condition at $a/h = 30$.

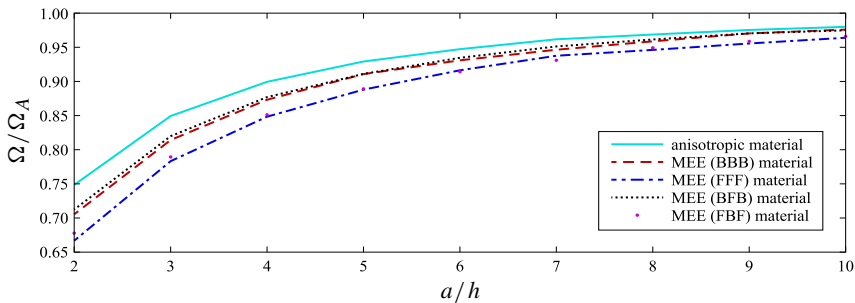


Figure 15. The relative differences of fundamental frequency of the CCFE plate compared to the thin plate limit for the five different material combinations as a function of a/h .

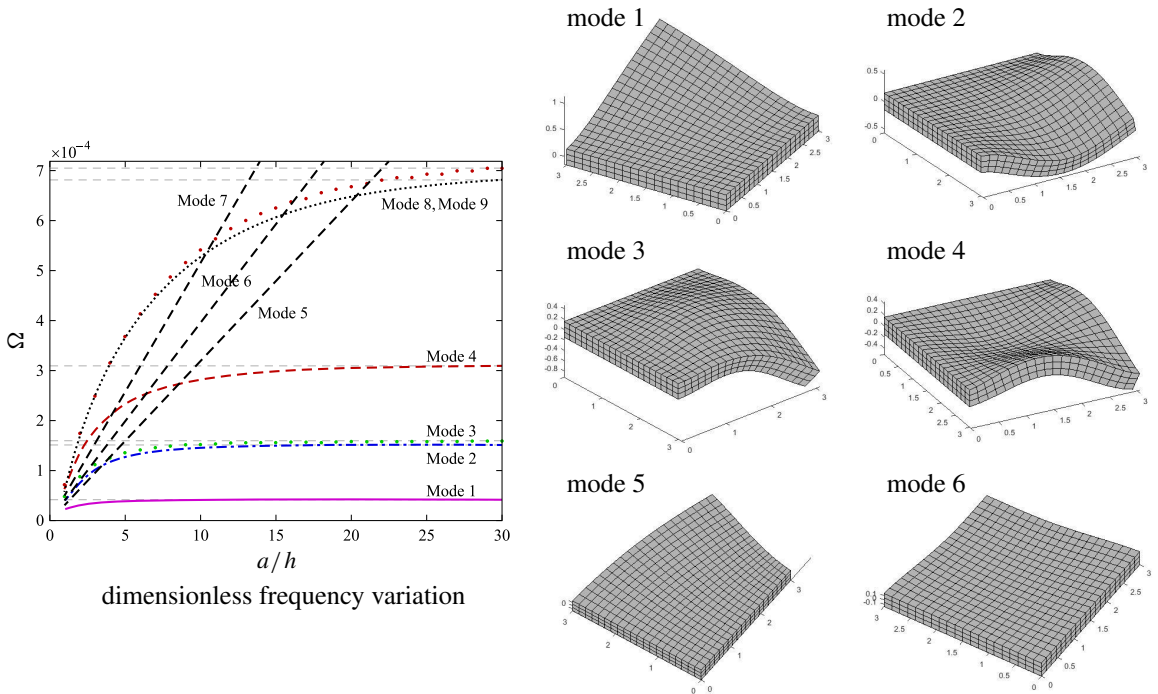


Figure 16. Frequency variation as a function of a/h and the first six mode shapes ($a/h = 10$) for the anisotropic elastic square CCFE plate.

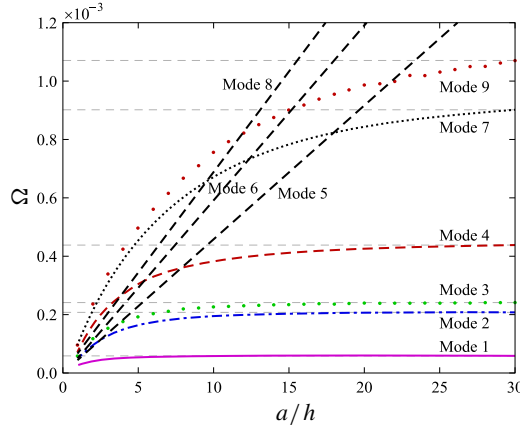


Figure 17. Dimensionless frequency variation as a function of a/h for the CCFB square BFB plate.

bending mode	hex	BBB	FFF	BFB	FBF
1	$4.36 \cdot 10^{-5}$	$1.01 \cdot 10^{-4}$	$6.63 \cdot 10^{-5}$	$6.08 \cdot 10^{-5}$	$7.12 \cdot 10^{-5}$
2	$1.53 \cdot 10^{-4}$	$3.50 \cdot 10^{-4}$	$2.28 \cdot 10^{-4}$	$2.10 \cdot 10^{-4}$	$2.44 \cdot 10^{-4}$
3	$1.60 \cdot 10^{-4}$	$3.99 \cdot 10^{-4}$	$2.64 \cdot 10^{-4}$	$2.42 \cdot 10^{-4}$	$2.82 \cdot 10^{-4}$
4	$3.11 \cdot 10^{-4}$	$7.24 \cdot 10^{-4}$	$4.67 \cdot 10^{-4}$	$4.38 \cdot 10^{-4}$	$5.00 \cdot 10^{-4}$
5	$6.82 \cdot 10^{-4}$	$1.50 \cdot 10^{-3}$	$9.43 \cdot 10^{-4}$	$9.01 \cdot 10^{-4}$	$1.02 \cdot 10^{-3}$
6	$7.06 \cdot 10^{-4}$	$1.73 \cdot 10^{-3}$	$1.12 \cdot 10^{-3}$	$1.07 \cdot 10^{-3}$	$1.20 \cdot 10^{-3}$

Table 13. Frequencies for homogeneous plates composed of five stacking sequences under CCFB condition at $a/h = 30$.

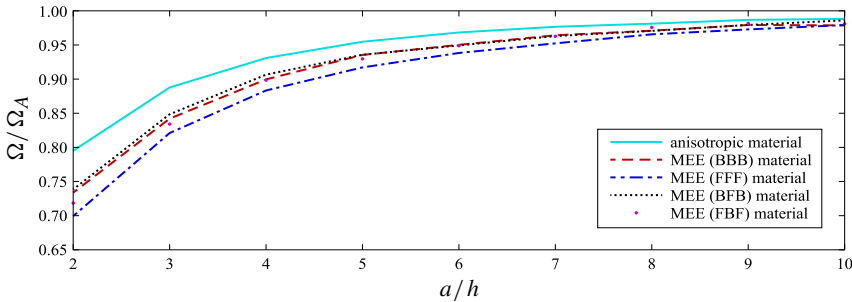


Figure 18. The relative differences of fundamental frequencies of the SFSF plate compared to the thin plate limit for the five different material combinations as a function of a/h .

free edges, are much smaller. With $a/h = 10$, the differences are within 10 percent. At $a/h = 20$, the percent differences are smaller than 2 percent. Table 14 gives the first six modes at $a/h = 30$.

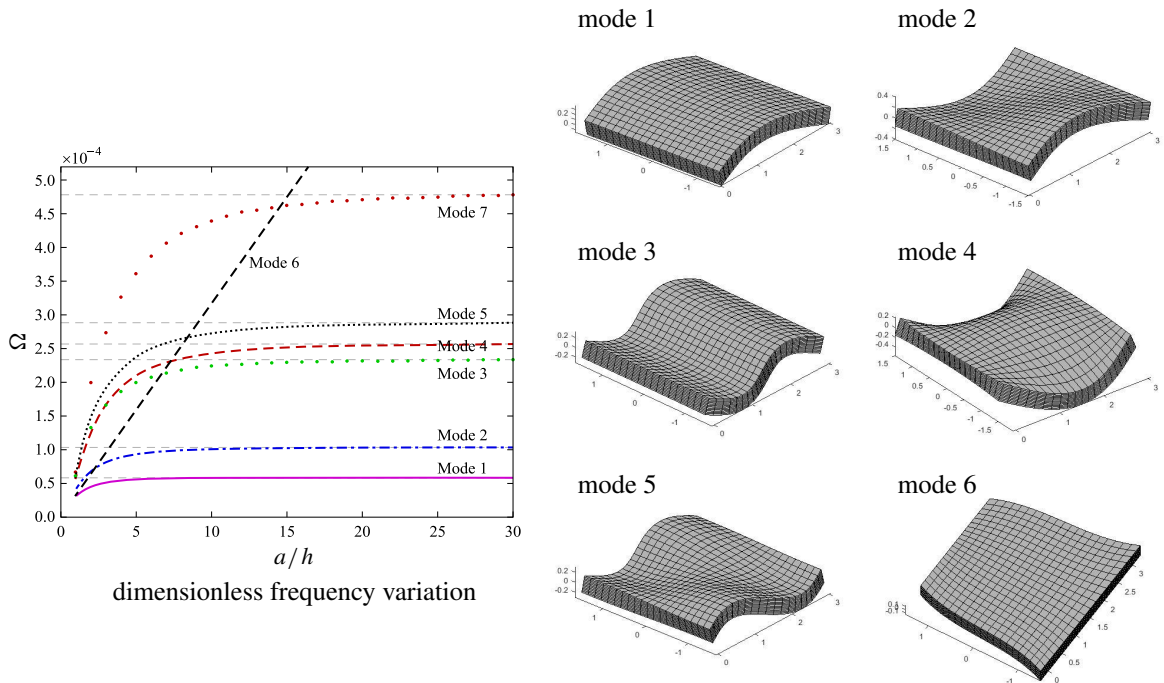


Figure 19. Frequency variation as a function of a/h and the first six mode shapes ($a/h = 10$) for the anisotropic elastic square SFSF plate.

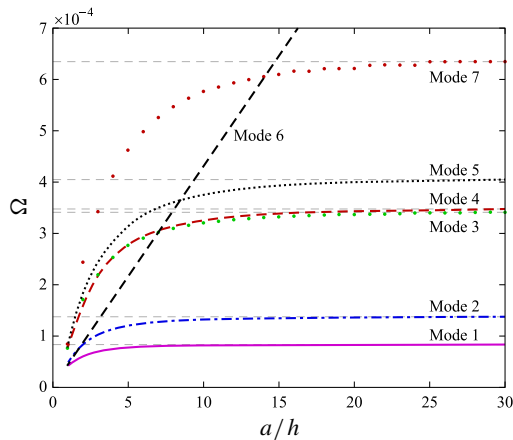


Figure 20. Dimensionless frequency variation as a function of a/h for the SFSF square BFB plate.

Conclusions

A discrete-layer model was used to approximate the natural frequencies of laminated isotropic and MEE plates under various boundary conditions. There are three primary conclusions related to this work:

- (1) The current DL model gives excellent agreement with most existing solutions for both isotropic and layered MEE plates. The main discrepancies arise for specific combinations of boundary conditions that have seen very little study in the literature.

bending mode	hex	BBB	FFF	BFB	FBF
1	$5.86 \cdot 10^{-5}$	$1.39 \cdot 10^{-4}$	$8.89 \cdot 10^{-5}$	$8.40 \cdot 10^{-5}$	$9.49 \cdot 10^{-5}$
2	$1.04 \cdot 10^{-4}$	$2.30 \cdot 10^{-4}$	$1.45 \cdot 10^{-4}$	$1.38 \cdot 10^{-4}$	$1.56 \cdot 10^{-4}$
3	$2.34 \cdot 10^{-4}$	$5.61 \cdot 10^{-4}$	$3.60 \cdot 10^{-4}$	$3.41 \cdot 10^{-4}$	$3.86 \cdot 10^{-4}$
4	$2.57 \cdot 10^{-4}$	$5.76 \cdot 10^{-4}$	$3.66 \cdot 10^{-4}$	$3.47 \cdot 10^{-4}$	$3.93 \cdot 10^{-4}$
5	$2.88 \cdot 10^{-4}$	$6.69 \cdot 10^{-4}$	$4.27 \cdot 10^{-4}$	$4.05 \cdot 10^{-4}$	$4.58 \cdot 10^{-4}$
6	$4.78 \cdot 10^{-4}$	$1.05 \cdot 10^{-3}$	$6.69 \cdot 10^{-4}$	$6.33 \cdot 10^{-4}$	$7.18 \cdot 10^{-4}$

Table 14. Frequencies for homogeneous plates composed of five stacking sequences under the SFSF condition at $a/h = 30$.

- (2) From all results and all cases considered in this study, the thin-plate limit of $a/h = 10$ does not give sufficient accuracy for a wide enough range of lamination schemes and boundary conditions. An a/h ratio of 20 gives a far better limit for using any thin-plate kinematic assumption.
- (3) The results contained herein for all boundary conditions can be used for purposes of comparison using other simplified theories of MEE plate behavior.

Appendix

$$K_{ij}^{11} = \int_V \left[C_{11} \frac{\partial \Psi_i^u}{\partial x} \frac{\partial \Psi_j^u}{\partial x} + C_{16} \left(\frac{\partial \Psi_i^u}{\partial x} \frac{\partial \Psi_j^u}{\partial y} + \frac{\partial \Psi_i^u}{\partial y} \frac{\partial \Psi_j^u}{\partial x} \right) + C_{55} \frac{\partial \Psi_i^u}{\partial z} \frac{\partial \Psi_j^u}{\partial z} + C_{66} \frac{\partial \Psi_i^u}{\partial y} \frac{\partial \Psi_j^u}{\partial y} \right] dV \quad (26)$$

$$K_{ij}^{12} = \int_V \left[C_{12} \frac{\partial \Psi_i^u}{\partial x} \frac{\partial \Psi_j^v}{\partial y} + C_{16} \frac{\partial \Psi_i^u}{\partial x} \frac{\partial \Psi_j^v}{\partial x} + C_{45} \frac{\partial \Psi_i^u}{\partial z} \frac{\partial \Psi_j^v}{\partial z} + C_{26} \frac{\partial \Psi_i^u}{\partial y} \frac{\partial \Psi_j^v}{\partial y} + C_{66} \frac{\partial \Psi_i^u}{\partial y} \frac{\partial \Psi_j^v}{\partial x} \right] dV \quad (27)$$

$$K_{ij}^{13} = \int_V \left[C_{13} \frac{\partial \Psi_i^u}{\partial x} \frac{\partial \Psi_j^w}{\partial z} + C_{45} \frac{\partial \Psi_i^u}{\partial z} \frac{\partial \Psi_j^w}{\partial y} + C_{55} \frac{\partial \Psi_i^u}{\partial z} \frac{\partial \Psi_j^w}{\partial x} + C_{36} \frac{\partial \Psi_i^u}{\partial y} \frac{\partial \Psi_j^w}{\partial z} \right] dV \quad (28)$$

$$K_{ij}^{14} = \int_V \left[e_{11} \frac{\partial \Psi_i^u}{\partial x} \frac{\partial \Psi_j^\phi}{\partial x} + e_{21} \frac{\partial \Psi_i^u}{\partial x} \frac{\partial \Psi_j^\phi}{\partial y} + e_{31} \frac{\partial \Psi_i^u}{\partial x} \frac{\partial \Psi_j^\phi}{\partial z} + e_{15} \frac{\partial \Psi_i^u}{\partial z} \frac{\partial \Psi_j^\phi}{\partial x} + e_{25} \frac{\partial \Psi_i^u}{\partial z} \frac{\partial \Psi_j^\phi}{\partial y} \right. \\ \left. + e_{35} \frac{\partial \Psi_i^u}{\partial z} \frac{\partial \Psi_j^\phi}{\partial z} + e_{16} \frac{\partial \Psi_i^u}{\partial y} \frac{\partial \Psi_j^\phi}{\partial x} + e_{26} \frac{\partial \Psi_i^u}{\partial y} \frac{\partial \Psi_j^\phi}{\partial y} + e_{36} \frac{\partial \Psi_i^u}{\partial y} \frac{\partial \Psi_j^\phi}{\partial z} \right] dV \quad (29)$$

$$K_{ij}^{15} = \int_V \left[q_{11} \frac{\partial \Psi_i^u}{\partial x} \frac{\partial \Psi_j^\psi}{\partial x} + q_{21} \frac{\partial \Psi_i^u}{\partial x} \frac{\partial \Psi_j^\psi}{\partial y} + q_{31} \frac{\partial \Psi_i^u}{\partial x} \frac{\partial \Psi_j^\psi}{\partial z} + q_{15} \frac{\partial \Psi_i^u}{\partial z} \frac{\partial \Psi_j^\psi}{\partial x} + q_{25} \frac{\partial \Psi_i^u}{\partial z} \frac{\partial \Psi_j^\psi}{\partial y} \right. \\ \left. + q_{35} \frac{\partial \Psi_i^u}{\partial z} \frac{\partial \Psi_j^\psi}{\partial z} + q_{16} \frac{\partial \Psi_i^u}{\partial y} \frac{\partial \Psi_j^\psi}{\partial x} + q_{26} \frac{\partial \Psi_i^u}{\partial y} \frac{\partial \Psi_j^\psi}{\partial y} + q_{36} \frac{\partial \Psi_i^u}{\partial y} \frac{\partial \Psi_j^\psi}{\partial z} \right] dV \quad (30)$$

$$K_{ij}^{22} = \int_V \left[C_{22} \frac{\partial \Psi_i^v}{\partial y} \frac{\partial \Psi_j^v}{\partial y} + C_{26} \left(\frac{\partial \Psi_i^v}{\partial y} \frac{\partial \Psi_j^v}{\partial x} + \frac{\partial \Psi_i^v}{\partial x} \frac{\partial \Psi_j^v}{\partial y} \right) + C_{44} \frac{\partial \Psi_i^v}{\partial z} \frac{\partial \Psi_j^v}{\partial z} + C_{66} \frac{\partial \Psi_i^v}{\partial x} \frac{\partial \Psi_j^v}{\partial x} \right] dV \quad (31)$$

$$K_{ij}^{23} = \int_V \left[C_{23} \frac{\partial \Psi_i^v}{\partial y} \frac{\partial \Psi_j^w}{\partial z} + C_{44} \frac{\partial \Psi_i^v}{\partial z} \frac{\partial \Psi_j^w}{\partial y} + C_{45} \frac{\partial \Psi_i^v}{\partial z} \frac{\partial \Psi_j^w}{\partial x} + C_{36} \frac{\partial \Psi_i^v}{\partial x} \frac{\partial \Psi_j^w}{\partial z} \right] dV \quad (32)$$

$$K_{ij}^{24} = \int_V \left[e_{12} \frac{\partial \Psi_i^v}{\partial y} \frac{\partial \Psi_j^\phi}{\partial x} + e_{22} \frac{\partial \Psi_i^v}{\partial y} \frac{\partial \Psi_j^\phi}{\partial y} + e_{32} \frac{\partial \Psi_i^v}{\partial y} \frac{\partial \Psi_j^\phi}{\partial z} + e_{14} \frac{\partial \Psi_i^v}{\partial z} \frac{\partial \Psi_j^\phi}{\partial x} + e_{24} \frac{\partial \Psi_i^v}{\partial z} \frac{\partial \Psi_j^\phi}{\partial y} \right. \\ \left. + e_{34} \frac{\partial \Psi_i^v}{\partial z} \frac{\partial \Psi_j^\phi}{\partial z} + e_{16} \frac{\partial \Psi_i^v}{\partial x} \frac{\partial \Psi_j^\phi}{\partial x} + e_{26} \frac{\partial \Psi_i^v}{\partial x} \frac{\partial \Psi_j^\phi}{\partial y} + e_{36} \frac{\partial \Psi_i^v}{\partial x} \frac{\partial \Psi_j^\phi}{\partial z} \right] dV \quad (33)$$

$$K_{ij}^{25} = \int_V \left[q_{12} \frac{\partial \Psi_i^v}{\partial y} \frac{\partial \Psi_j^\psi}{\partial x} + q_{22} \frac{\partial \Psi_i^v}{\partial y} \frac{\partial \Psi_j^\psi}{\partial y} + q_{32} \frac{\partial \Psi_i^v}{\partial y} \frac{\partial \Psi_j^\psi}{\partial z} + q_{14} \frac{\partial \Psi_i^v}{\partial z} \frac{\partial \Psi_j^\psi}{\partial x} + q_{24} \frac{\partial \Psi_i^v}{\partial z} \frac{\partial \Psi_j^\psi}{\partial y} \right. \\ \left. + q_{34} \frac{\partial \Psi_i^v}{\partial z} \frac{\partial \Psi_j^\psi}{\partial z} + q_{16} \frac{\partial \Psi_i^v}{\partial x} \frac{\partial \Psi_j^\psi}{\partial x} + q_{26} \frac{\partial \Psi_i^v}{\partial x} \frac{\partial \Psi_j^\psi}{\partial y} + q_{36} \frac{\partial \Psi_i^v}{\partial x} \frac{\partial \Psi_j^\psi}{\partial z} \right] dV \quad (34)$$

$$K_{ij}^{33} = \int_V \left[C_{33} \frac{\partial \Psi_i^w}{\partial z} \frac{\partial \Psi_j^w}{\partial z} + C_{44} \frac{\partial \Psi_i^w}{\partial y} \frac{\partial \Psi_j^w}{\partial y} \right. \\ \left. + C_{45} \frac{\partial \Psi_i^w}{\partial y} \frac{\partial \Psi_j^w}{\partial x} + C_{45} \frac{\partial \Psi_i^w}{\partial x} \frac{\partial \Psi_j^w}{\partial y} + C_{55} \frac{\partial \Psi_i^w}{\partial x} \frac{\partial \Psi_j^w}{\partial x} \right] dV \quad (35)$$

$$K_{ij}^{34} = \int_V \left[e_{13} \frac{\partial \Psi_i^w}{\partial z} \frac{\partial \Psi_j^\phi}{\partial x} + e_{23} \frac{\partial \Psi_i^w}{\partial z} \frac{\partial \Psi_j^\phi}{\partial y} + e_{33} \frac{\partial \Psi_i^w}{\partial z} \frac{\partial \Psi_j^\phi}{\partial z} + e_{14} \frac{\partial \Psi_i^w}{\partial y} \frac{\partial \Psi_j^\phi}{\partial x} + e_{24} \frac{\partial \Psi_i^w}{\partial y} \frac{\partial \Psi_j^\phi}{\partial y} \right. \\ \left. + e_{34} \frac{\partial \Psi_i^w}{\partial y} \frac{\partial \Psi_j^\phi}{\partial z} + e_{15} \frac{\partial \Psi_i^w}{\partial x} \frac{\partial \Psi_j^\phi}{\partial x} + e_{25} \frac{\partial \Psi_i^w}{\partial x} \frac{\partial \Psi_j^\phi}{\partial y} + e_{35} \frac{\partial \Psi_i^w}{\partial x} \frac{\partial \Psi_j^\phi}{\partial z} \right] dV \quad (36)$$

$$K_{ij}^{44} = \int_V \left[-\epsilon_{11} \frac{\partial \Psi_i^\phi}{\partial x} \frac{\partial \Psi_j^\phi}{\partial x} - \epsilon_{22} \frac{\partial \Psi_i^\phi}{\partial y} \frac{\partial \Psi_j^\phi}{\partial y} - \epsilon_{33} \frac{\partial \Psi_i^\phi}{\partial z} \frac{\partial \Psi_j^\phi}{\partial z} \right] dV \quad (37)$$

$$K_{ij}^{55} = \int_V \left[-\mu_{11} \frac{\partial \Psi_i^\psi}{\partial x} \frac{\partial \Psi_j^\psi}{\partial x} - \mu_{22} \frac{\partial \Psi_i^\psi}{\partial y} \frac{\partial \Psi_j^\psi}{\partial y} - \mu_{33} \frac{\partial \Psi_i^\psi}{\partial z} \frac{\partial \Psi_j^\psi}{\partial z} \right] dV \quad (38)$$

References

- [Abromowitz and Stegun 1966] M. Abromowitz and I. A. Stegun (editors), *Handbook of mathematical functions, with formulas, graphs, and mathematical tables*, Dover, New York, 1966.
- [Chen et al. 2005] W. Q. Chen, K. Y. Lee, and H. J. Ding, “On free vibration of non-homogeneous transversely isotropic magneto-electro-elastic plates”, *J. Sound Vib.* **279**:1 (2005), 237–251.
- [Chen et al. 2007] J. Chen, H. Chen, E. Pan, and P. R. Heyliger, “Modal analysis of magneto-electro-elastic plates using the state-vector approach”, *J. Sound Vib.* **304**:3 (2007), 722–734.
- [Chen et al. 2014] J. Y. Chen, P. R. Heyliger, and E. Pan, “Free vibration of three-dimensional multilayered magneto-electro-elastic plates under combined clamped/free boundary conditions”, *J. Sound Vib.* **333**:17 (2014), 4017–4029.
- [Demarest 1971] H. H. Demarest, Jr., “Cube-resonance method to determine the elastic constants of solids”, *J. Acoust. Soc. Am.* **49**:3B (1971), 768–775.
- [Eer Nisse 1967] E. P. Eer Nisse, “Variational method for electroelastic vibration analysis”, *IEEE Transactions on Sonics and Ultrasonics* **14**:4 (1967), 153–159.

- [Heyliger 2000] P. Heyliger, “Traction-free vibration of layered elastic and piezoelectric rectangular parallelepipeds”, *J. Acoust. Soc. Am.* **107**:3 (2000), 1235–1245.
- [Hjelmstad 1997] K. D. Hjelmstad, *Fundamentals of structural mechanics*, 1st ed., Prentice Hall, Upper Saddle River, NJ, 1997.
- [Kondaiah et al. 2012] P. Kondaiah, K. Shankar, and N. Ganesan, “Studies on magneto-electro-elastic cantilever beam under thermal environment”, *Coupled systems mechanics* **1**:2 (2012), 205–217.
- [Liew et al. 1993] K. M. Liew, Y. Xiang, and S. Kitipornchai, “Transverse vibration of thick rectangular plates, I: comprehensive sets of boundary conditions”, *Comput. Struct.* **49**:1 (1993), 1–29.
- [Ohno 1976] I. Ohno, “Free vibration of a rectangular parallelepiped crystal and its application to determination of elastic constants of orthorhombic crystals”, *J. Phys. Earth* **24**:4 (1976), 355–379.
- [Pan and Heyliger 2002] E. Pan and P. R. Heyliger, “Free vibrations of simply supported and multilayered magneto-electro-elastic plates”, *J. Sound Vib.* **252**:3 (2002), 429–442.
- [Rao 2007] S. S. Rao, *Vibration of continuous systems*, Wiley, 2007.
- [Reddy and Phan 1985] J. Reddy and N. Phan, “Stability and vibration of isotropic, orthotropic and laminated plates according to a higher-order shear deformation theory”, *J. Sound Vib.* **98**:2 (1985), 157–170.
- [Srinivas et al. 1970] S. Srinivas, C. V. Joga Rao, and A. K. Rao, “Some results from an exact analysis of thick laminates in vibration and buckling”, *J. Appl. Mech. (ASME)* **37** (1970), 868–870.
- [Szilard 1974] R. Szilard, *Theory and analysis of plates*, Prentice-Hall, Englewood Cliffs, N.J., 1974.
- [Tiersten 1969] H. F. Tiersten, *Linear piezoelectric plate vibrations*, Springer, New York, 1969.
- [Ugural and Fenster 1995] A. C. Ugural and S. K. Fenster, *Advanced strength and applied elasticity*, 3rd ed., Prentice-Hall, Englewood Cliffs, NJ, 1995.
- [Vel and Batra 2000] S. S. Vel and R. C. Batra, “Three-dimensional analytical solution for hybrid multilayered piezoelectric plates”, *J. Appl. Mech. (ASME)* **67**:3 (2000), 558–567.
- [Vel et al. 2004] S. S. Vel, R. Mewer, and R. Batra, “Analytical solution for the cylindrical bending vibration of piezoelectric composite plates”, *Int. J. Solids Struct.* **41**:5-6 (2004), 1625–1643.
- [Wang et al. 2003] J. Wang, L. Chen, and S. Fang, “State vector approach to analysis of multilayered magneto-electro-elastic plates”, *Int. J. Solids Struct.* **40**:7 (2003), 1669–1680.
- [Whitney 1987] J. M. Whitney, *Structural analysis of laminated composite plates*, CRC Press, 1987.

Received 12 Jan 2017. Revised 4 Apr 2017. Accepted 19 May 2017.

CHAO JIANG: chao@rams.colostate.edu

Department of Civil and Environmental Engineering, Colorado State University, Fort Collins, CO, United States

PAUL R. HEYLIGER: prh@engr.colostate.edu

Department of Civil and Environmental Engineering, Colorado State University, Fort Collins, CO, United States

JOURNAL OF MECHANICS OF MATERIALS AND STRUCTURES

msp.org/jomms

Founded by Charles R. Steele and Marie-Louise Steele

EDITORIAL BOARD

ADAIR R. AGUIAR	University of São Paulo at São Carlos, Brazil
KATIA BERTOLDI	Harvard University, USA
DAVIDE BIGONI	University of Trento, Italy
YIBIN FU	Keele University, UK
IWONA JASIUK	University of Illinois at Urbana-Champaign, USA
MITSUTOSHI KURODA	Yamagata University, Japan
C. W. LIM	City University of Hong Kong
THOMAS J. PENCE	Michigan State University, USA
GIANNI ROYER-CARFAGNI	Università degli studi di Parma, Italy
DAVID STEIGMANN	University of California at Berkeley, USA
PAUL STEINMANN	Friedrich-Alexander-Universität Erlangen-Nürnberg, Germany

ADVISORY BOARD

J. P. CARTER	University of Sydney, Australia
D. H. HODGES	Georgia Institute of Technology, USA
J. HUTCHINSON	Harvard University, USA
D. PAMPLONA	Universidade Católica do Rio de Janeiro, Brazil
M. B. RUBIN	Technion, Haifa, Israel

PRODUCTION production@msp.org

SILVIO LEVY Scientific Editor


Cover photo: Mando Gomez, www.mandolux.com

See msp.org/jomms for submission guidelines.

JoMMS (ISSN 1559-3959) at Mathematical Sciences Publishers, 798 Evans Hall #6840, c/o University of California, Berkeley, CA 94720-3840, is published in 10 issues a year. The subscription price for 2017 is US \$615/year for the electronic version, and \$775/year (+\$60, if shipping outside the US) for print and electronic. Subscriptions, requests for back issues, and changes of address should be sent to MSP.

JoMMS peer-review and production is managed by EditFLOW[®] from Mathematical Sciences Publishers.

PUBLISHED BY

 **mathematical sciences publishers**
nonprofit scientific publishing

<http://msp.org/>

© 2017 Mathematical Sciences Publishers

B-splines collocation for plate bending eigenanalysis	CHRISTOPHER G. PROVATIDIS	353
Shear capacity of T-shaped diaphragm-through joints of CFST columns	BIN RONG, RUI LIU, RUOYU ZHANG, SHUAI LIU and APOSTOLOS FAFITIS	373
Polarization approximations for elastic moduli of isotropic multicomponent materials	DUC CHINH PHAM, NGUYEN QUYET TRAN and ANH BINH TRAN	391
A nonlinear micromechanical model for progressive damage of vertebral trabecular bones	EYASS MASSARWA, JACOB ABOUDI, FABIO GALBUSERA, HANS-JOACHIM WILKE and RAMI HAJ-ALI	407
Nonlocal problems with local Dirichlet and Neumann boundary conditions	BURAK AKSOYLU and FATIH CELIKER	425
Optimization of Chaboche kinematic hardening parameters by using an algebraic method based on integral equations	LIU SHIJIE and LIANG GUOZHU	439
Interfacial waves in an A/B/A piezoelectric structure with electro-mechanical imperfect interfaces	M. A. REYES, J. A. OTERO and R. PÉREZ-ÁLVAREZ	457
Fully periodic RVEs for technological relevant composites: not worth the effort!	KONRAD SCHNEIDER, BENJAMIN KLUSEMANN and SWANTJE BARGMANN	471
Homogenization of a Vierendeel girder with elastic joints into an equivalent polar beam	ANTONIO GESUALDO, ANTONINO IANNUZZO, FRANCESCO PENTA and GIOVANNI PIO PUCILLO	485
Highly accurate noncompatible generalized mixed finite element method for 3D elasticity problems	GUANGHUI QING, JUNHUI MAO and YANHONG LIU	505
Thickness effects in the free vibration of laminated magneto-electroelastic plates	CHAO JIANG and PAUL R. HEYLIGER	521
Localized bulging of rotating elastic cylinders and tubes	JUAN WANG, ALI ALTHOBAITI and YIBIN FU	545